AGU PUBLICATIONS

Geophysical Research Letters

RESEARCH LETTER
10.1002/2016GL069938

Key Points:
- Records of SO_2 flux emissions from Etna's individual vents allow capturing shifts in volcanic activity
- Vent-resolved SO_2 flux time series provide constraints on geometry of the shallow plumbing system
- Vent-resolved SO_2 flux time series demonstrate SO_2 flux increase precursory to paroxysmal (lava fountaining) activity

Correspondence to:
R. D'Aleo,
roberto.daleo01@unipa.it

Citation:
D'Aleo, R., M. Bitetto, D. Delle Donne, G. Tamburello, A. Battaglia, M. Coltelli, D. Patanè, M. Prestifilippo, M. Sciotto, and A. Aiuppa (2016), Spatially resolved SO_2 flux emissions from Mt Etna, *Geophys. Res. Lett.*, *43*, 7511–7519, doi:10.1002/2016GL069938.

Received 7 JUN 2016
Accepted 12 JUL 2016
Accepted article online 14 JUL 2016
Published online 30 JUL 2016

Spatially resolved SO_2 flux emissions from Mt Etna

R. D'Aleo[1], M. Bitetto[1], D. Delle Donne[1], G. Tamburello[1], A. Battaglia[1], M. Coltelli[2], D. Patanè[2], M. Prestifilippo[2], M. Sciotto[2], and A. Aiuppa[1,3]

[1]DiSTeM, Università di Palermo, Palermo, Italy, [2]Istituto Nazionale di Geofisica e Vulcanologia, Sezione di Catania, Catania, Italy, [3]Istituto Nazionale di Geofisica e Vulcanologia, Sezione di Palermo, Palermo, Italy

Abstract We report on a systematic record of SO_2 flux emissions from individual vents of Etna volcano (Sicily), which we obtained using a permanent UV camera network. Observations were carried out in summer 2014, a period encompassing two eruptive episodes of the New South East Crater (NSEC) and a fissure-fed eruption in the upper Valle del Bove. We demonstrate that our vent-resolved SO_2 flux time series allow capturing shifts in activity from one vent to another and contribute to our understanding of Etna's shallow plumbing system structure. We find that the fissure eruption contributed ~50,000 t of SO_2 or ~30% of the SO_2 emitted by the volcano during the 5 July to 10 August eruptive interval. Activity from this eruptive vent gradually vanished on 10 August, marking a switch of degassing toward the NSEC. Onset of degassing at the NSEC was a precursory to explosive paroxysmal activity on 11–15 August.

1. Introduction

The advent of increasingly sophisticated imaging techniques [*Kern et al*., 2015] has recently prompted a revolution in our ability to study volcanic gas emissions. Ground-based observations via UV cameras [*Mori and Burton*, 2006], in particular, have granted acquisition of volcanic SO_2 flux time series of unprecedented temporal and spatial resolution, thus paving the way to a variety of novel volcano-monitoring applications (see *Burton et al*. [2015] for a review). Importantly, UV cameras can allow examining "fast" degassing processes at high rate and in real time, therefore opening the way to integration of geophysical and volcanic gas data sets into multidisciplinary models of volcanic explosions [*Dalton et al*., 2010; *Nadeau et al*., 2011; *Tamburello et al*., 2012; *Waite et al*., 2013; *Pering et al*., 2015], passive degassing [*Tamburello et al*., 2013], and lava lake dynamics [*Nadeau et al*., 2015].

One additional advantage of UV cameras is that at least in principle, these are suited to adaptation to fully automated, permanent systems for long-term SO_2 flux monitoring [*Burton et al*., 2015; *Kern et al*., 2015]. Within the context of the Framework programme 7-European Research Council-funded Project *BRIDGE* (http://www.bridge.unipa.it/), we recently deployed two stand-alone UV camera systems on the flanks of Mt. Etna volcano, one of the strongest punctual sources of volcanic gas worldwide [*Oppenheimer et al*., 2011]. Etna has one of the longest and most complete records of volcanic SO_2 flux [*Caltabiano et al*., 2004]. However, the majority of the available data are spectroscopically sensed from relatively remote measurement sites, located several kilometers away from the volcano's summit. In such conditions, any transient degassing signal (e.g., from puffing behavior and/or discrete explosions) is lost during atmospheric transport, the contribution of individual vents cannot be resolved, and the temporal resolution of observations is typically in the approximately tens of minutes range [*Salerno et al*., 2009].

Here we report on results obtained from the BRIDGE network, in a period encompassing the summer 2014 eruptive episodes of Etna volcano. We show that our observations contribute spatially and temporally resolved SO_2 flux time series that, when interpreted in tandem with independent volcanological and geophysical (seismic tremor and infrasound data) information, allow to fully interpret and understand the time-changing degassing and eruptive behavior of the volcano. We demonstrate, in particular, that transition from one degassing/eruptive mode/site to another, a recurrent process on Etna [*Allard et al*., 2006; *Marchetti et al*., 2009; *Cannata et al*., 2011a; *Patanè et al*., 2008, 2013], can be fully captured from the UV camera.

2. Materials and Methods

The SO_2 flux data were collected with a network of permanent, fully autonomous UV cameras run by University of Palermo (Figure 1). The network includes two stand-alone UV camera systems installed at La

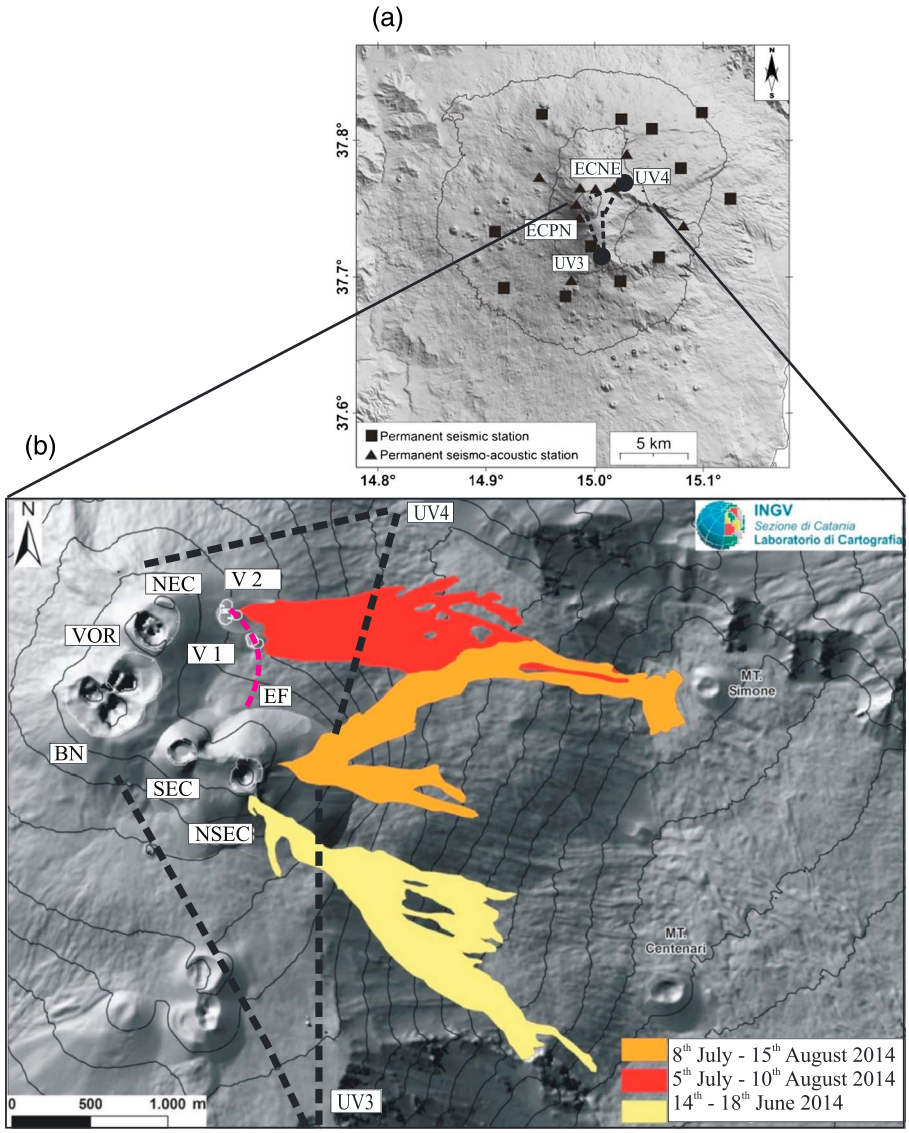

Figure 1. (a) Digital map of Mt. Etna showing the location of the permanent UV camera systems (UV3 and UV4; with their field of views) and of the geophysical multiparametric stations (ECNE and ECPN) of which data are used in the present study. (b) A detail of Figure 1a, with Etna's five summit craters (NSEC: New Southeast; SEC; Southeast; BN: Bocca Nuova; VOR: Voragine; NEC: Northeast). The summer 2014 Eruptive Fissure (EF) and Vents (V1: vent of EF phase 1; and V2: vent EF Phase 2) and the June–August 2014 lava flow fields are also indicated (redrawn from *De Beni et al.* [2015] and INGV-OE monitoring reports; see www.ct.ingv.it).

Montagnola (UV3), 3.5 km from the New South East Crater (NSEC), and at Pizzi Deneri (UV4), 2 km from the North East Crater (NEC) (Figure 1). The two UV camera systems are designed to separately resolve degassing activity from Etna's summit craters NSEC and NEC (Figure 2). We specifically designed the network to also capture the degassing from any eruptive fissure (EF) opened on the upper Etna's Eastern flank. This is the upper portion of the Valle del Bove area (Figure 1) where eruptive activity has systematically been concentrating since 2004 [*Behncke et al.*, 2006, 2014]. Our SO_2 flux time series do not account for degassing from Bocca Nuova and Voragine craters (Figure 1) and therefore should not be considered as representative of the total volcano's SO_2 budget.

At both UV3 and UV4, the UV camera system is equipped with the following: (i) two JAI CM 140 GR cameras, with 10 bit digitization and 1392 × 1040 pixels. Each camera mounts a Uka Optics UV lens with ~37° field of view and a band-pass filter from Edmund Optics (full width at half maximum: 10 nm), centered at either

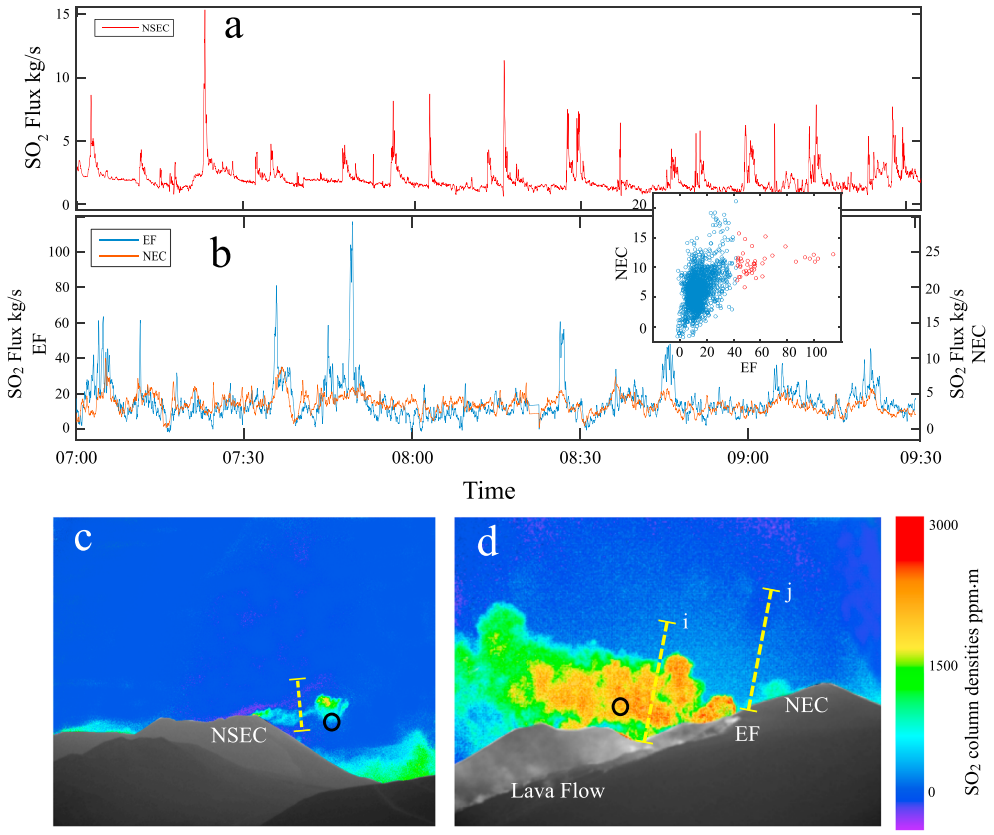

Figure 2. (a) An example of 2.5 h long SO_2 flux time series of the NSEC, taken from UV3 on 9 July 2014. (c) A representative pseudocolor image of the plume, demonstrating the cameras' field of view, is shown. The largest (>5 kg/s) SO_2 flux pulses correspond to Strombolian explosions. (b) An example of 2.5 h long acquisitions from UV4, taken on 14 August 2014. (d) The plumes of both the NEC and the eruptive fracture (EF) were simultaneously contained in the cameras' field of view (see pseudocolor image). From this, the SO_2 flux contributions from the two distinct gas sources were resolved from ICA time series obtained along two different plume's cross sections (dashed yellow lines in Figure 2d), one (labeled "*j*") relative to SO_2 flux contributions from the NEC only and the other (labeled "*i*") corresponding to gas contributions from NEC + EF. This procedure contributed two SO_2 flux time series (in which the EF flux was calculated as the difference between the EF + NEC flux and the NEC flux) that exhibited a high level of temporal coherence (see scatterplot in the inset). Since the SO_2 flux oscillations at the EF are 5–10 times higher than at the NEC, we consider it unlikely that the correlation between the two time series is an effect of our calculation routine. In both pseudocolor images (Figures 2c and 2d), the empty circles indicate the Field of View of the spectrometer used for camera calibration.

310 nm or 330 nm; (ii) an Ocean optics USB2000+ UV Spectrometer; and (iii) a Dlink DCS 3010 visible IP camera. The cameras, controlled by either a mini-PC Jetway (UV4) or a computer server (UV3), capture sequential images of the plume at ~0.5 Hz rate during 6 h long measurement intervals each day. Each set of coacquired images, from both UV cameras, is processed using the methodology of *Kantzas et al.* [2010] through the Vulcamera software [*Tamburello et al.*, 2011] to calculate an absorbance for each camera pixel. This is converted into an SO_2 column amount using simultaneous UV spectrometer readings as outlined in *Lübcke et al.* [2013] and finally into integrated column amounts (ICAs) along a plume cross section. To calculate SO_2 flux time series examples of which are given in Figure 2, the obtained ICA time series were combined with high-temporal records of plume transport speed. These were derived at ~1 Hz using an optical flow subroutine using the Lukas/Kanade algorithm [*Bruhn et al.*, 2005; *Peters et al.*, 2015], integrated in Vulcamera.

Our SO_2 flux data set was integrated with seismic and infrasonic data recorded by the permanent networks run by the Istituto Nazionale di Geofisica e Vulcanologia, Osservatorio Etneo (INGV-OE). Seismic stations used to investigate volcanic tremor are equipped with broadband (40 s corner period), three-component Nanometrics™ Trillium seismometers acquiring at a sampling rate of 100 Hz (Figure 1). Seismic amplitudes were obtained by calculating RMS (root-mean-square) envelope over 1 min long nonoverlapping time

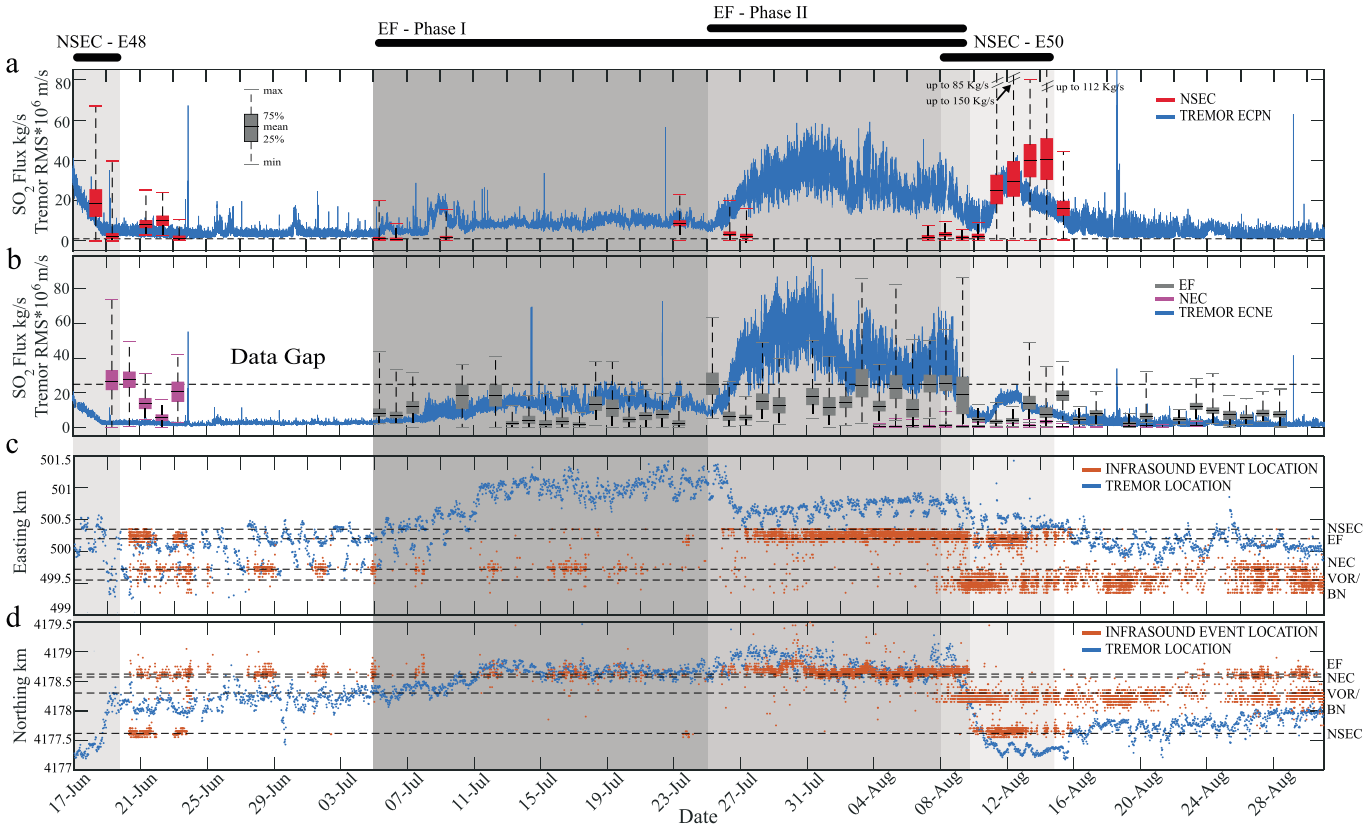

Figure 3. Temporal record (17 June to 31 August) of SO_2 flux emissions from (a) the NSEC and (b) the NEC and the July–August 2014 Eruptive Fissure (EF). For each measurement day and degassing vent, the vertical bars show mean, minimum (min), maximum (max), and interquartile (25–75%) range of the SO_2 flux. The blue-colored lines stand for volcanic tremor amplitude (RMS × 10^6) from recorded at ECPN (in Figure 3a) and ECNE (in Figure 3b) stations (see Figure 1 for their location). (c) The locations of the centroid of volcanic tremor (blue) and infrasound events (red) are shown, highlighting activity switch between different sources/vents. Centroids of the volcanic tremor sources were obtained by means of a grid search location method based on spatial amplitude distribution of seismic signal filtered in the frequency band 0.5–5.5 Hz (for details see *Di Grazia et al.* [2006], *Patanè et al.* [2008], and *Cannata et al.* [2013]). In order to locate infrasound event sources, we applied a grid search method based on the composite use of semblance and brightness functions (see *Cannata et al.* [2011b, 2013] for details). On the upper side, solid bars mark the eruptive activity of NCSE (episodes E48 and E50 in *De Beni et al.* [2015]) and two phases of EF.

windows at ECNE (Figure 3b) and ECPN stations (Figure 3a). The infrasonic permanent network, in 2014, was made up of nine stations, three equipped with Monacor condenser microphones (sensitivity of 80 mV/Pa in the 1–20 Hz infrasonic band) and the others with G.R.A.S.S. 40AN microphones (sensitivity of 50 mV/Pa and flat response in the 0.3–20,000 Hz band). In order to investigate eruption dynamics and the interconnection between craters involved in the 2014 summer eruption, we located volcanic tremor and infrasound events extracted from the continuous signal [*Di Grazia et al.*, 2006; *Patanè et al.*, 2008; *Cannata et al.*, 2011b, 2013].

Volcanic activity was recorded by video surveillance camera network of INGV-OE (www.ct.ingv.it/en/web-cam-etna-en.html) operating both in visible, with standard and 5 MP video resolutions, and thermal bands. Cameras located at La Montagnola, in the same shelter hosting UV3 camera, and Mt. Cagliato on the middle eastern flank at about 7 km from the summit area were able to record any change of the eruptive activity that occurred in the summer of 2014.

3. Volcanic Activity

The SO_2 flux observations we report on in this work were taken between 17 June and 31 August 2014, when both UV3 and UV4 systems were operating (Figure 3). This temporal window encompasses two eruptive episodes of the NSEC, on 14–18 June (therefore only partially covered by our measurements) and 8–15 August. The first episode, referred to as E48 in *De Beni et al.* [2015], started with a 1 month long prelude phase, in which mild Strombolian activity with weak ash emissions increased in frequency/intensity. This was followed

by a 4 day long paroxysmal phase, with intense Strombolian explosions to lava fountaining that formed lava flow traveling on the cone's eastern flank toward the Valle del Bove (Figure 1) (www.ct.ingv.it and *De Beni et al*. [2015]). After 3 days of scanty explosions from NSEC and 2 weeks without any summit activity, an eruptive fissure (EF) opened in the Valle del Leone, the upper side of Valle del Bove, on the east flank of the NEC (Figure 1). According to *De Beni et al*. [2015], the EF activity was fed by a NW-SE-trending fractures system, departing from the NSEC (Figure 1). The EF eruption consisted of two phases (I: 5–25 July; II: 25 July to 10 August) that occurred from two distinct but closely spaced vents, at 3000 m and 3090 m elevation (Figure 1). Both phases were characterized by emplacement of a compound lava flow field that covered a wide area of the Valle del Leone, during a strong spattering/Strombolian activity at the vents, which were particularly intense during phase II. The EF activity gradually vanished during 8–10 August, in tandem with resuming of activity at the NSEC (episode E50). On late 10 August Strombolian explosions became intense forming the first lava flow. The paroxysmal phase occurred on 11–15 August, when lava fountaining fed both an ash-rich plume and a vigorous lava flow traveling toward the northern side of the Valle del Bove.

4. Results

Figure 2 shows examples of two 2.5 h long UV camera acquisitions from (a) UV3 and (b) UV4. The plots demonstrate the usual structure of high-rate Etna's SO_2 flux time series, characterized by the repetition (periods of tens to thousands of seconds) of small-amplitude ($<$5 kg/s) gas flux oscillations produced by emission of distinct gas pulses or "puffs" [*Tamburello et al*., 2013]. Superimposed on this "puffing" degassing style are, at both the NSEC (Figure 2a) and EF (Figure 2b), stronger ($>$5 kg/s) SO_2 pulsations, typically lasting tens of seconds to minutes and corresponding to individual Strombolian explosions or, more frequently, sequences of closely spaced Strombolian events (Figure 2).

In the attempt to explore the temporal evolution of degassing behavior at each target, we calculated, for each measurement day and crater, the mean SO_2 flux value and the interquartile ranges. We remind that our mean daily values are in fact representative of only 6 h of observations. These exhibited large variations during our 10 week observation period (Figure 3).

The NSEC (Figure 3a) contributed little to the total SO_2 budget during the most part of the observational period and was characterized by SO_2 emission below the instrumental detection limit ($<$1 kg/s) during its periods of quiescence. In contrast, the NSEC was the strongest SO_2 source (among those analyzed here) during its 11–15 August eruptive episode, with mean SO_2 fluxes of 16.0 to 44.4 kg/s, and a peak emission of 150 kg/s during the major (paroxysmal) eruptive phases on 13 August. In the same 11–15 August interval, source locations of both seismic tremor and infrasound events (Figure 3c) confirm that eruptive/degassing activity was concentrating at the NSEC. Interestingly enough, the NSEC SO_2 emissions were also detectable (range, 2–20 kg/s) between 5–9 July and 23–27 July, e.g., at onset of both eruptive episodes of the July 2014 EF, and, even more importantly, in the days (7–10 August) prior to the NSEC paroxysmal activity of 11–15 August. These preparoxysmal gas detections at the NSEC were accompanied by a concomitant shift in seismic tremor centroid and infrasound event locations, from the EF toward NSEC, during 9–10 August (Figure 3c).

The SO_2 degassing regime of the EF (Figure 3b) was clearly captured by our network since eruption onset on 5 July. The daily means of the EF SO_2 flux ranged from 2.1 to 26.6, and daily peak emissions varied from 11.5 to 86.4 kg/s. SO_2 emissions were typically higher during episode II (25 July to 10 August) than in episode I (5–25 July), in agreement with distinct volcanic tremor RMS amplitudes (Figures 3a and 3b). The initial phases of EF activity were accompanied by a weak and gradual increase of seismic amplitude, and a migration of volcanic tremor centroids, from central craters toward EF area (Figure 3c). In contrast, more evident amplitude variations occurred on 25 July (start of EF phase II), when RMS amplitude sharply increased (Figures 3a and 3b). Intense explosive activity at EF during phase II (25 July to 10 August) is revealed by infrasound events, which had sources located in the area of EF (Figure 3c). Notably, the EF SO_2 emissions attenuated on 10 August, just 1 day before eruptive activity switched to the NSEC (Figure 4).

SO_2 degassing at the NEC (Figure 3b) was substantially reduced (daily means of 1.2–4.2 kg/s) during the EF activity, at least compared to the preeruptive period, e.g., end of June daily means: 5.7–27.7 kg/s; peak SO_2 fluxes: 16.1–75 kg/s. After opening of the EF on 5 July, the NEC contributed only ~20% of the EF + NEC flux.

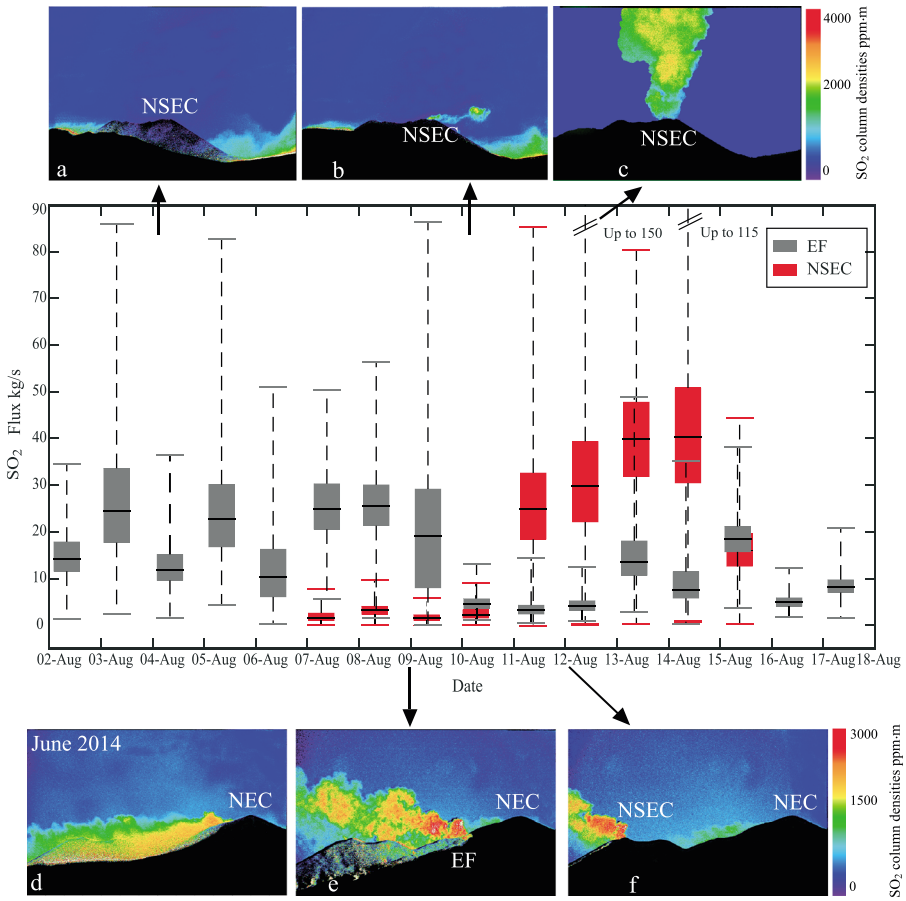

Figure 4. Detail (2 August to 18 August) of SO_2 flux time series from the NSEC and EF, demonstrating activity switch on 10–11 August. The paroxysmal NSEC activity (11–15 August) was preceded by four consecutive days of precursory mild (but detectable) SO_2 emissions.

Yet notwithstanding, daily records (e.g., Figure 2b) systematically showed a high level of coherence (e.g., simultaneous gas variations) between EF and NEC throughout the entire eruption duration.

5. Discussion

UV cameras contribute SO_2 flux time series of unprecedented high spatial and temporal resolution and therefore open the way to investigating novel aspects of volcano degassing regime. At Etna, a >30 year long SO_2 flux record is available from use of the COrrelation SPECtrometer (COSPEC) [*Caltabiano et al.*, 1994, 2004] and, more recently, from continuous UV scanning spectrometers of the FLux Automatic MEasurements (FLAME) network [*Salerno et al.*, 2009] using the Differential Optical Absorption Spectroscopy (DOAS) technique [*Galle et al.*, 2003]. In contrast to such distal (>5 km from degassing vents) "bulk plume" measurements, near-vent observations of individual crater's SO_2 flux have remained very sporadic and limited in number [*McGonigle et al.*, 2005; *Aiuppa et al.*, 2008, 2011; *La Spina et al.*, 2010]. The Etna's four summit craters have diverse degassing/erupting behaviors and often exhibit fast transitions in activity style, with frequent switches from one vent to another over timescales of hours/days [*Allard et al.*, 2006]. As such, vent-resolved SO_2 flux measurements are needed to fully interpret, and eventually predict, the volcano's behavior.

Our study here attempts at a systematic characterization of SO_2 emissions from Etna's individual craters/eruptive vents. While we admit that gas emissions from Etna's central craters do also require careful scrutiny, we here specifically target gas emissions from the eastern side of the volcanic summit (Figure 1), where eruptions have been clustering since 2004 (www.ct.ingv.it and *Branca and Del Carlo* [2005] and *Behncke et al.* [2006, 2014]).

The summer 2014 example shows that SO_2 emissions from an eruptive fissure can successfully be monitored over time using UV cameras (Figure 3b). The daily averaged SO_2 emissions from the 2014 EF eruption ranged between 2.1 and 26.6 kg/s and, if extrapolated over the entire eruption duration (≈36 days), imply a cumulative released SO_2 mass of 50,000 t. This corresponds to ≈ 30% of the total SO_2 mass released by Etna during the same temporal interval (considering an average total SO_2 flux of ≈ 3000 tons/day in July–August 2014, as measured by the FLAME network of INGV-OE; www.ct.ingv.it). We conclude that during eruptive periods, active degassing at the fissures contributes a nonmarginal fraction of the volcano's total SO_2 budget. This result has typically been difficult to prove from traditional spectroscopic observations made from distal locations [*Caltabiano et al*., 2004], where volatiles contributed from a single fissure are dispersed within the "bulk plume" and mixed with volatiles derived from the summit craters.

SO_2 emissions from the NEC virtually ceased during the 2014 EF activity (Figure 3b). A data acquisition gap (from 23 June to 15 July) prevents us from establishing the exact timing of the SO_2 drop at NEC. Still, no SO_2 emission was detected from the NEC during most part of the EF eruptive episode (until 5 August), and the SO_2 flux was detectable but low (≤4.2 kg/s) until late August. We interpret the drastic reduction of the NEC SO_2 emissions, combined with the temporal coherence observed in the NEC and EF time series (Figure 2b), as an evidence for the two systems being structurally connected. We propose that opening of the EF in early July drained magma/gas normally circulating in the NEC feeding conduit system. Interestingly, a similar link between the NEC conduit system and an eruptive fissure was proposed based on geophysical data by *Sciotto et al*. [2013] for the 2008–2009 eruption, which occurred in similar area [*Bonaccorso et al*., 2011].

The appearance of SO_2 at the NSEC, in concomitance with onset of both EF eruptive phases (Figure 3a), suggests a structural link between these two systems as well. We propose a mechanism in which the EF eruption was triggered by magma intrusion along the NW-SE trending dyke, irradiating from the NEC, and which tip eventually intersected the NSEC plumbing system (Figure 1b). The centroids of seismic tremor, located at about 2.5–3 km above sea level, suggest that dyke intrusion propagated at a very shallow depth. Some level of structural interconnection between EF and NSEC is also supported by Figure 4, where degassing activity at the former is seen to vanish (on 10 August) as the latter becomes active (during 11–16 August). This activity switch, evident in the gas record (Figure 4), is also captured as a rapid shift in the centroid of seismic tremor and infrasound event locations, from the EF area toward NSEC crater (Figure 3c). We caution that while a connection between EF and NEC/NSEC conduits is supported by our SO_2 and volcanic tremor data, additional (independent) evidence for this hydraulic link needs to be established. We cannot rule out that our observations merely reflect ascent of gas, rather than magma, through interconnected chimneys opening as the Etna's upper plumbing system pressurizes.

Our observations also allow characterizing the SO_2 degassing behavior of the Etna's NSEC (Figures 3a and 4). This pyroclastic cone, developed over a series of collapse pits formed on the eastern flank of the SEC cone during 2004–2009, has shown an unusually fast growth and eruptive rate in 2011–2014. Fifty eruptive episodes, including lava fountaining episodes, Strombolian activity, and lava flows have been recognized at NSEC by *Behncke et al*. [2014] and *De Beni et al*. [2015], making this crater the current largest source of volcanic hazard on the volcano [*Spampinato et al*., 2015]. No gas flux information has been reported for the NSEC until this study. We show here that the NSEC exhibits no detectable SO_2 flux (<1 kg/s) during quiescence but becomes a substantial source of gas (with peak emissions up to 150 kg/s) during its paroxysmal eruptive phases (Figures 3a and 4). Importantly, low but detectable (2–3 kg/s) SO_2 flux emissions from the NSEC were detected for four consecutive days (7–10 August) prior to onset of the paroxysmal phase of 11–15 August (Figure 4). Such preparoxysm gas detections at the NSEC appear to anticipate the shift in volcanic tremor centroid and infrasound event location, from the EF toward NSEC, which were clearly visible only on 9–10 August (Figure 3c). Our gas observations are promising, but more work is needed to understand their implications for a robust, gas-based early-warning system of NSEC eruptions.

6. Conclusions

In this work, we took advantage of the high spatial (~5 m) and temporal (~1 Hz) resolution of the UV camera to systematically investigate SO_2 gas emissions from Etna's individual vents. Our vent-resolved SO_2 flux time

series suggest rapid (hours/days) switch in degassing activity from one active vent to another, that implies a geometry of the Etna's shallow plumbing system with interconnections between summit vents (NEC and NSEC) and with (EF) summit eruptive fissure.

We find that the 2014 EF contributed a substantial (~30%) fraction of the total volcano SO_2 budget and altered the usual magma/gas circulation in the summit craters' shallow feeding conduits. The SO_2 emissions from the NEC were, consequently, strongly reduced. Our SO_2 flux records also indicate that the NSEC contributed little or no gas to the quiescent Etna's emissions in summer 2014. SO_2 degassing activity reactivated at the NSEC in the days prior to its eruptions and intensified as volcanic activity escalated toward paroxysmal phases. We conclude that UV cameras open new prospects for identifying short-term gas flux variations prior to paroxysmal Etna eruptions.

Acknowledgments
The research leading to these results has received funding from the European Research Council under the European Union's Seventh Framework Programme (FP7/2007/2013)/ERC grant agreement 305377 (Principal Investigator: A.A.). We acknowledge E. Privitera, Director of INGV-OE, and F. Ciancitto for logistic support during UV camera deployments.

References

Aiuppa, A., G. Giudice, S. Gurrieri, M. Liuzzo, M. Burton, T. Caltabiano, A. J. S. McGonigle, G. Salerno, H. Shinohara, and M. Valenza (2008), Total volatile flux from Mount Etna, *Geophys. Res. Lett.*, *35*, L24302, doi:10.1029/2008GL035871.

Aiuppa, A., H. Shinohara, G. Tamburello, G. Giudice, M. Liuzzo, and R. Moretti (2011), Hydrogen in the gas plume of an open-vent volcano, Mount Etna, Italy, *J. Geophys. Res.*, *116*, B10204, doi:10.1029/2011JB008461.

Allard, P., B. Behncke, S. D'Amico, M. Neri, and S. Gambino (2006), Mount Etna 1993–2005: Anatomy of an evolving eruptive cycle, *Earth Sci. Rev.*, *78*(1–2), 85–114, doi:10.1016/j.earscirev.2006.04.002.

Behncke, B., M. Neri, E. Pecora, and V. Zanon (2006), The exceptional activity and growth of the Southeast Crater, Mount Etna (Italy), between 1996 and 2001, *Bull. Volcanol.*, *69* (2), 149–173, doi:10.1007/s00445-006-0061-x.

Behncke, B., S. Branca, R. A. Corsaro, E. De Beni, L. Miraglia, and C. Proietti (2014), The 2011–2012 summit activity of Mount Etna: Birth, growth and products of the new SE crater, *J. Volcanol. Geotherm. Res.*, *270*, 10–21, doi:10.1016/j.jvolgeores.2013.11.012.

Bonaccorso, A., A. Bonforte, S. Calvari, C. Del Negro, G. Di Grazia, G. Ganci, M. Neri, A. Vicari, and E. Boschi (2011), The initial phases of the 2008–2009 Mount Etna eruption: A multidisciplinary approach for hazard assessment, *J. Geophys. Res.*, *116*, B03203, doi:10.1029/2010JB007906.

Branca, S., and P. Del Carlo (2005), Types of eruptions of Etna volcano AD 1670–2003: Implications for short-term eruptive behaviour, *Bull. Volcanol.*, *67*(8), 732–742, doi:10.1007/s00445-005-0412-z.

Bruhn, A., J. Weickert, and C. Schnörr (2005), Lucas/Kanade meets Horn/Schunck: Combining local and global optic flow methods, *Int. J. Comput. Vis.*, *61*(3), 211–231, doi:10.1023/B:VISI.0000045324.43199.43.

Burton, M. R., G. G. Salerno, L. D'Auria, T. Caltabiano, F. Murè, and R. Maugeri (2015), SO_2 flux monitoring at Stromboli with the new permanent INGV SO_2 camera system: A comparison with the FLAME network and seismological data, *J. Volcanol. Geotherm. Res.*, *300*, 95–102, doi:10.1016/j.jvolgeores.2015.02.006.

Caltabiano, T., R. Romano, and G. Budetta (1994), SO_2 flux measurements at Mount Etna (Sicily), *J. Geophys. Res.*, *99*, 12,809–12,819, doi:10.1029/94JD00224.

Caltabiano, T., M. Burton, S. Giammanco, P. Allard, N. Bruno, F. Murè, and R. Romano (2004), Volcanic gas emissions from the summit craters and flanks of Mt. Etna, 1987–2000, in *Mt. Etna: Volcano Laboratory*, *Geophys. Monogr. Ser.*, vol. 143, edited by A. Bonaccorso et al., pp. 111–128, AGU, Washington, D. C., doi:10.1029/143GM08.

Cannata, A., P. Montalto, M. Aliotta, C. Cassisi, A. Pulvirenti, E. Privitera, and D. Patanè (2011a), Clustering and classification of infrasonic events at Mount Etna using pattern recognition techniques, *Geophys. J. Int.*, *185*(1), 253–264, doi:10.1111/j.1365-246X.2011.04951.x.

Cannata, A., M. Sciotto, L. Spampinato, and L. Spina (2011b), Insights into explosive activity at eruptive fissure closely-spaced eruptive vents using infrasound signals: Example of Mt. Etna 2008 eruption, *J. Volcanol. Geotherm. Res.*, *208*, 1–11, doi:10.1016/j.jvolgeores.2011.09.003.

Cannata, A., G. Di Grazia, M. Aliotta, C. Cassisi, P. Montalto, and D. Patanè (2013), Monitoring seismo-volcanic and infrasonic signals at volcanoes: Mt. Etna case study, *Pure Appl. Geophys.*, *170*, 1751–1771, doi:10.1007/s00024-012-0634-x.

Dalton, M. P., G. P. Waite, I. M. Watson, and P. A. Nadeau (2010), Multiparameter quantification of gas release during weak Strombolian eruptions at Pacaya Volcano, Guatemala, *Geophys. Res. Lett.*, *37*, L09303, doi:10.1029/2010GL042617.

De Beni, E., B. Behncke, S. Branca, I. Nicolosi, R. Carluccio, F. D'Ajello Caracciolo, and M. Chiappini (2015), The continuing story of Etna's new Southeast Crater (2012–2014): Evolution and volume calculations based on field surveys and aerophotogrammetry, *J. Volcanol. Geotherm. Res.*, *303*, 175–186, doi:10.1016/j.jvolgeores.2015.07.021.

Di Grazia, G., S. Falsaperla, and H. Langer (2006), Volcanic tremor location during the 2004 Mount Etna lava effusion, *Geophys. Res. Lett.*, *33*, L04304, doi:10.1029/2005GL025177.

Galle, B., C. Oppenheimer, A. Geyer, A. J. S. McGonigle, M. Edmonds, and L. A. Horrocks (2003), A miniaturised ultraviolet spectrometer for remote sensing of SO_2 fluxes: A new tool for volcano surveillance, *J. Volcanol. Geotherm. Res.*, *119*, 241–254, doi:10.1016/S0377-0273(02)00356-6.

Kantzas, E. P., A. J. S. McGonigle, G. Tamburello, A. Aiuppa, and R. G. Bryant (2010), Protocols for UV camera volcanic SO_2 measurements, *J. Volcanol. Geotherm. Res.*, *94*, 55–60, doi:10.1016/j.jvolgeores.2010.05.003.

Kern, C., J. Sutton, T. Elias, L. Lee, K. Kamibayashi, L. Antolik, and C. Werner (2015), An automated SO_2 camera system for continuous, real-time monitoring of gas emissions from Kīlauea Volcano's summit Overlook Crater, *J. Volcanol. Geotherm. Res.*, *300*, 81–94, doi:10.1016/j.jvolgeores.2014.12.004.

Kern, C., et al. (2015), Intercomparison of SO_2 camera systems for imaging volcanic gas plumes, *J. Volcanol. Geotherm. Res.*, *300*, 22–36, doi:10.1016/j.jvolgeores.2014.08.026.

La Spina, A., M. Burton, and G. G. Salerno (2010), Unravelling the processes controlling gas emissions from the central and northeast craters of Mt. Etna, *J. Volcanol. Geotherm. Res.*, *198*(3–4), 368–376, doi:10.1016/j.jvolgeores.2010.09.018.

Lübcke, P., N. Bobrowski, S. Illing, C. Kern, J. M. Alvarez Nieves, L. Vogel, J. Zielcke, H. Delgado Granados, and U. Platt (2013), On the absolute calibration of SO_2 cameras, *Atmos. Meas. Tech.*, *6*, 677–696, doi:10.5194/amt-6-677-2013.

Marchetti, E., M. Ripepe, G. Ulivieri, S. Caffo, and E. Privitera (2009), Infrasonic evidences for branched conduit dynamics at Mt. Etna volcano, Italy, *Geophys. Res. Lett.*, *36*, L19308, doi:10.1029/2009GL040070.

McGonigle, A. J. S., S. Inguaggiato, A. Aiuppa, A. R. Hayes, and C. Oppenheimer (2005), Accurate measurement of volcanic SO_2 flux: Determination of plume transport speed and integrated SO_2 concentration with a single device, *Geochem. Geophys. Geosyst.*, *6*, Q02003, doi:10.1029/2004GC000845.

Mori, T., and M. Burton (2006), The SO_2 camera: A simple, fast and cheap method for ground-based imaging of SO_2 in volcanic plumes, *Geophys. Res. Lett.*, *33*, L24804, doi:10.1029/2006GL027916.

Nadeau, P. A., L. P. Jose, and G. P. Waite (2011), Linking volcanic tremor, degassing, and eruption dynamics via SO_2 imaging, *Geophys. Res. Lett.*, *38*, L01304, doi:10.1029/2010GL045820.

Nadeau, P. A., C. A. Werner, G. P. Waite, S. A. Carn, I. D. Brewer, T. Elias, A. J. Sutton, and C. Kern (2015), Using SO_2 camera imagery and seismicity to examine degassing and gas accumulation at Kīlauea Volcano, May 2010, *J. Volcanol. Geotherm. Res.*, *300*, 70–80, doi:10.1016/j.jvolgeores.2014.12.005.

Oppenheimer, C., B. Scaillet, and R. S. Martin (2011), Sulfur degassing from volcanoes: Source conditions, surveillance, plume chemistry and earth system impacts, *Rev. Mineral. Geochem.*, *73*, 363–421.

Patanè, D., G. Di Grazia, A. Cannata, P. Montalto, and E. Boschi (2008), Shallow magma pathway geometry at Mt. Etna volcano, *Geochem. Geophys. Geosyst.*, *9*, Q12021, doi:10.1029/2008GC002131.

Patanè, D., et al. (2013), Insights into magma and fluid transfer at Mount Etna by a multiparametric approach: A model of the events leading to the 2011 eruptive cycle, *J. Geophys. Res. Solid Earth*, *118*, 3519–3539, doi:10.1002/jgrb.50248.

Pering, T. D., G. Tamburello, A. J. S. McGonigle, A. Aiuppa, M. R. James, S. J. Lane, M. Sciotto, A. Cannata, and D. Patanè (2015), Dynamics of mild Strombolian activity on Mt. Etna, *J. Volcanol. Geotherm. Res.*, *300*, 103–111, doi:10.1016/j.jvolgeores.2014.12.013.

Peters, N., A. Hoffmann, T. Barnie, M. Herzog, and C. Oppenheimer (2015), Use of motion estimation algorithms for improved flux measurements using SO_2 cameras, *J. Volcanol. Geotherm. Res.*, *300*, 58–69, doi:10.1016/j.jvolgeores.2014.08.031.

Salerno, G. G., M. R. Burton, C. Oppenheimer, T. Caltabiano, D. Randazzo, N. Bruno, and V. Longo (2009), Three-years of SO_2 flux measurements of Mt. Etna using an automated UV scanner array: Comparison with conventional traverses and uncertainties in flux retrieval, *J. Volcanol. Geotherm. Res.*, *183*(1–2), 76–83, doi:10.1016/j.jvolgeores.2009.02.013.

Sciotto, M., A. Cannata, S. Gresta, E. Privitera, and L. Spina (2013), Seismic and infrasound signals at Mt. Etna: Modeling the North-East crater conduit and its relation with the 2008–2009 eruption feeding system, *J. Volcanol. Geotherm. Res.*, *254*, 53–68, doi:10.1016/j.jvolgeores.2012.12.024.

Spampinato, L., M. Sciotto, A. Cannata, F. Cannavò, A. La Spina, M. Palano, G. G. Salerno, E. Privitera, and T. Caltabiano (2015), Multiparametric study of the February–April 2013 paroxysmal phase of Mt. Etna new South-East crater, *Geochem. Geophys. Geosyst.*, *16*, 1932–1949, doi:10.1002/2015GC005795.

Tamburello, G., E. P. Kantzas, A. J. S. McGonigle, and A. Aiuppa (2011), Vulcamera: A program for measuring volcanic SO_2 using UV cameras, *Ann. Geophys.*, *54*, 2, doi:10.4401/ag-5181.

Tamburello, G., A. Aiuppa, E. P. Kantzas, A. J. S. McGonigle, and M. Ripepe (2012), Passive vs. active degassing modes at an open-vent volcano (Stromboli, Italy), *Earth Planet. Sci. Lett.*, *359*, 106–116, doi:10.1016/j.epsl.2012.09.050.

Tamburello, G., A. Aiuppa, A. J. S. McGonigle, P. Allard, A. Cannata, G. Giudice, E. P. Kantzas, and T. D. Pering (2013), Periodic volcanic degassing behaviour: The Mount Etna example, *Geophys. Res. Lett.*, *40*, 4818–4822, doi:10.1002/grl.50924.

Waite, G. P., P. A. Nadeau, and J. J. Lyons (2013), Variability in eruption style and associated very long period events at Fuego volcano, Guatemala, *J. Geophys. Res. Solid Earth*, *118*, 1526–1533, doi:10.1002/jgrb.50075.